Batteries & Supercaps

Research Article
doi.org/10.1002/batt.202200219

Chemistry Europe
European Chemical Societies Publishing

www.batteries-supercaps.org

VIP *Very Important Paper*

Special Collection

Controlling Horizontal Growth of Zinc Platelet by OP-10 Additive for Dendrite-Free Aqueous Zinc-Ion Batteries

Dong Han,[a] Tianjiang Sun,[a] Haihui Du,[a] Qiaoran Wang,[a] Shibing Zheng,[a] Tao Ma,[a] and Zhanliang Tao*[a]

Rechargeable zinc-ion batteries based on aqueous electrolytes are advantageous in terms of being environmentally friendly, safe and low cost. However, the problems of zinc dendrites and irreversible by-products on the Zn metal surface during the charging and discharging processes limit its practical application. Herein, octenyl phenol polyoxyethylene ether-10 (OP-10) with an oxygen-rich chain is used as an electrolyte additive to significantly improve the stability of the Zn anode. With an ultralow addition content of about 0.1 wt%, the OP-10 can not only promote the uniform deposition of Zn^{2+} by adjusting the growth orientation of the (002) crystal plane of Zn but also alleviate side-reaction on the metal surface. Thus, the Zn//Zn cell is stable for more than 800 hours at 1 mA cm^{-2}, and the Zn//Cu cell has a Coulombic efficiency of up to 99.80%. Further, the Zn//$V_2O_5 \cdot 1.6H_2O$ battery exhibits outstanding cycle stability over 1000 cycles (maintain 92.12% at 10 C), which is much superior to pure $ZnSO_4$ electrolyte. OP-10 not only reduces cost but also increases battery energy density, which is more in line with the modification idea of "small dose and large effect" of additives.

Introduction

Aqueous zinc-ion batteries (AZIBs) are rechargeable batteries that are promising for future development, for mass storage energy systems due to less assembling costs, materials, and better safer operation.[1–3] In addition, the used Zn metal anode possesses a high specific capacity and volumetric capacity (820 mAh g^{-1} and 5,854 mAh cm^{-3}), high crustal abundance, and low redox potential [−0.76 V vs. standard hydrogen electrode (SHE)].[4] In recent years, the research of cathode materials in AZIBs has been carried out in full swing, but many experiments showed that the zinc anode undergoes surface side reactions and dendrite growth which are the main factors that limit the performance of the AZIBs. Due to the presence of the tip effect, the initially formed zinc protrusion shows stronger electric field intensity[5] and zinc ions tend to deposit at the tip of zinc protrusions,[6] compared with alkali metals such as lithium and sodium, zinc metal has higher Young's modulus and mechanical strength, further growth of dendrites may cause separator piercing and internal short circuit.[7,8] Meanwhile, the side reaction (like parasitic hydrogen evolution reaction (HER)) and by-products (like $Zn_4SO_4(OH)_6 \cdot 4H_2O$, ZnO, and other insulating products) produced with water and dissolved oxygen in the electrolyte during the process of zinc deposition, which is also one of the important reasons to limit the cycle performance of AZIBs.[9–11] Thus, it is urgent to protect the zinc anode to achieve robust AZIBs.[12,13]

Various strategies are being used for improving zinc anode performance from the aspects of the surface modification technology of the zinc electrode,[5,14–16] the optimization of the zinc internal structure,[17,18] and novel functional separator.[11,19,20] For instance, Li et al. designed zincophilic and spatial traps through a host of porous Co-embedded carbon cages, which allows dendrite-free conduct with outstanding kinetics.[21] Zhang et al. designed a composite gel electrolyte (TA-SA) from a highly-confined tannic acid (TA) modified sodium alginate (SA), it efficiently suppresses Zn side reactions and dendrite growth.[22] Among them, the optimization of electrolytes is an effective and simple strategy, which includes using electrolyte additives and, selecting the less-water and anhydrous electrolytes with high salinity, gel, and others.[21–27] Although the less-water and anhydrous electrolytes reduce the side reactions caused by free water, their high cost and ionic conductivity lose the advantages of the aqueous electrolytes themselves. By contrast, the electrolyte additives with the unique merit of "small dose and high efficiency", can significantly improve the battery performance without increasing the production cost and production difficulty. For example, Xu et al. found that if diethyl ether is added to 3 M $Zn(CF_3SO_3)_2$ electrolyte in certain amounts, it improves Zn//MnO_2 battery performance. This is based on the principle that molecules' polarity causes their preferential absorbance on initially produced small-sized zinc protrusions. The small zinc protrusion generated high local electric field is shielded by adsorbed ether molecule layer, thus further blocking the electro-deposition of Zn-ions on these protrusions.[28] Sun et al. significantly improved the number of cycles and capacity retention of the battery by adding cheap

[a] D. Han, T. Sun, H. Du, Q. Wang, S. Zheng, T. Ma, Prof. Z. Tao
Key Laboratory of Advanced Energy Materials Chemistry
Ministry of Education, Renewable Energy Conversion and Storage Center,
College of Chemistry
Haihe Laboratory of Sustainable Chemical Transformations
Nankai University
Tianjin 300071, P. R. China
E-mail: taozhl@nankai.edu.cn

Supporting information for this article is available on the WWW under https://doi.org/10.1002/batt.202200219

Special Collection *An invited contribution to a Special Collection dedicated to Aqueous Electrolyte Batteries*

and common glucose to the $ZnSO_4$ electrolyte.[29] However, the optimal usage of electrolyte additives is so high that electrolyte viscosity is increased, and the ionic conductivity and reaction kinetics of the solution is reduced (for example, the additive mentioned above was 1–10% organic matter[28–32]). Therefore, it is an urgent need to find an optimal additive with a lower proportion to improve the battery performance on the premise of not reducing the ionic conductivity of the aqueous electrolyte and fast reaction kinetics.

Organic molecules can regulate Zn-ions interfacial distribution and also affect the zinc metal's crystal growth orientation. Some organic molecule additives like polyethylene-glycol (PEG), thiourea (TU), and sodium dodecyl sulfate (SDS), have been reported to improve Zn-anode by altering zinc plating's crystal orientation and reducing its corrosion.[33] For example, the PEG additive is capable of making (103) and (002) planes dominant, suggesting that dendrite formation may not be due to crystal growth on the (002) plane being nearly horizontal with the electrode surface.[34] The PEG additive eliminates high local velocity regions, and decreases the average flow velocity, thereby extending the over potential range and allowing a stable electrode position. In contrast, some additives, such as cetyltrimethylammonium bromide (CTAB), are unfavorable as they can induce (101) plane and decrease (103) and (002) planes; thus, CTAB does not allow dendrite formation.[33]

Generally, small quantities of additive species will preferentially adsorb onto and accumulate near surface protrusions and thereby stabilize the electrodeposition in a regime below a critical flux.[35,36] Appropriate molecules for guiding Zn-crystal growth orientation are important. Herein, OP-10 (octenyl phenol polyoxyethylene ether-10, hereinafter referred to as OP-10), a common emulsifier, is used as the electrolyte additive of AZIBs for the first time. It is worth noting that the OP-10 with an ultralow dosage of 0.1 wt% can significantly improve the performance of the zinc metal anode for AZIBs after being added to 2 M ($mol\,L^{-1}$) of $ZnSO_4$ solution. A large number of zinc-philic groups of OP-10 increase the nucleation sites, which can homogenize the transport of Zn^{2+} cations toward the electrode surface, making the Zn (002) planes dominant and greatly reducing dendrite growth and by-product formation. The cycle life of the Zn//Zn symmetrical cell system assembled with $ZnSO_4$ electrolyte containing OP-10 additive is more than 800 hours at 1 $mA\,cm^{-2}$ with 1 $mAh\,cm^{-2}$, and the Coulombic efficiency of the Zn//Cu cell is as high as 99.80% at 1 $mA\,cm^{-2}$ with 1 $mAh\,cm^{-2}$. Further, the capacity retention of the Zn//$V_2O_5\cdot1.6H_2O$ battery in $ZnSO_4$ electrolyte containing 0.1 wt% OP-10 additive is still maintaining 92.12% after 1000 cycles at 10 C (5890 $mA\,g^{-1}$, 1 C = 589 $mA\,g^{-1}$), which is far better than pure $ZnSO_4$ electrolyte (maintain 58.34% at 10 C).

Results and Discussion

The zinc foil is easy to form a porous and loose corrosion layer in the acid electrolyte, which makes the electrolyte penetrate the zinc foil, resulting in continuous corrosion and reducing the service life of the battery. Figure 1(a) shows zinc foils that were immersed in 2 M $ZnSO_4$ electrolyte with and without OP-10 for two weeks, respectively. The surface of zinc foils was uneven after immersing for two weeks in pure $ZnSO_4$ electrolyte, showing obvious corrosion traces, while the zinc foils immersed in $ZnSO_4$ with 0.1 wt% OP-10 electrolyte were relatively smooth and flat without obvious morphological changes. The corrosion resistance of the electrolyte with OP-10 additive is further quantitatively investigated by Tafel curves as shown in Figure 1(b). Compared to the pure $ZnSO_4$ electrolyte, the corrosion potential of $ZnSO_4$ with OP-10 electrolyte increased from −0.021 to −0.011 V (vs. Zn^{2+}/Zn) with the added amount of OP-10 increasing from 0.05 wt% to 0.5 wt%, with less tendency for electrochemical corrosion reactions. In addition, for evaluating the rate at which self-corrosion reactions occur, the corrosion current density (i_{corr}) remains to be a direct factor. Here, the i_{corr} of $ZnSO_4$ with 0.1 wt% OP-10 electrolyte (0.28 $mA\,cm^{-2}$) is greatly decreased than that of pure $ZnSO_4$ electrolyte (0.62 $mA\,cm^{-2}$), which can be linked with OP-10 adsorption on the surface of the Zn-foil. Benefiting from the rich electronegative oxygen-containing groups of OP-10 (Figure S1), a large number of zinc-philic groups are adsorbed on the surface of the zinc foil to inhibit the corrosion of the zinc anode.[33] It's worth noting that with the continued addition of OP-10, the i_{corr} of the electrolyte decreases slowly (Figure 1c). Meanwhile, the hydrogen evolution potential decreased significantly with the added amount of OP-10 increasing (Figure 1d). This extensive electrochemical window is advantageous for increasing the available voltage range of the batteries, decreasing hydrogen evolution reaction, and reducing the risks of swelling and even leakage of AZIBs. These findings show that the presence of OP-10 additive effectively suppresses anodic corrosion and hydrogen evolution reactions. Electrochemical quartz crystal microbalance (EQCM) is used to calculate the change of adsorption quality based on the change of crystal oscillation frequency during adsorption or deposition on a quartz crystal oscillation plate.[37] A layer of zinc was deposited on the surface of the quartz sheet, and then $ZnSO_4$ with OP-10 electrolyte was added to EQCM and placed in a vacuum condition. The adsorption mass on the Zn-foil surface gradually increased within one hour and finally floated around 90 $\mu g\,cm^{-2}$, indicating that the adsorption of OP-10 on the surface of zinc foil may reach saturation (Figure 1e). The electrochemical test can also prove these. The overpotential of nucleation advances from 101.1 mV to 137.7 mV post OP-10 addition into pure $ZnSO_4$ electrolyte (Figure S2), revealing it has the function to slow Zn deposition.

The wettability between electrolyte and electrode is important for Zn deposition behavior. The electrode surface that has good wettability can efficiently retain electrolytes and promote uniform Zn-ions distribution on the interface. The contact angle between zinc and $ZnSO_4$ with OP-10 electrolyte is significantly lower than that between zinc and pure $ZnSO_4$ electrolyte, the electrolyte contact angles of Zn anode at 0 s and 120 s reduced in the pure $ZnSO_4$ electrolyte (89.7° and 82.8°) > with 0.05 wt% OP-10 (78.7° and 70.5°) > with 0.1 wt% OP-10 (61.1° and 49.5°) > with 0.2 wt% OP-10 (58.6° and 48.5°) > with 0.5 wt% OP-10 (53.8° and 46°) (Figures 1f and S3),

Research Article
doi.org/10.1002/batt.202200219
Chemistry Europe
European Chemical Societies Publishing

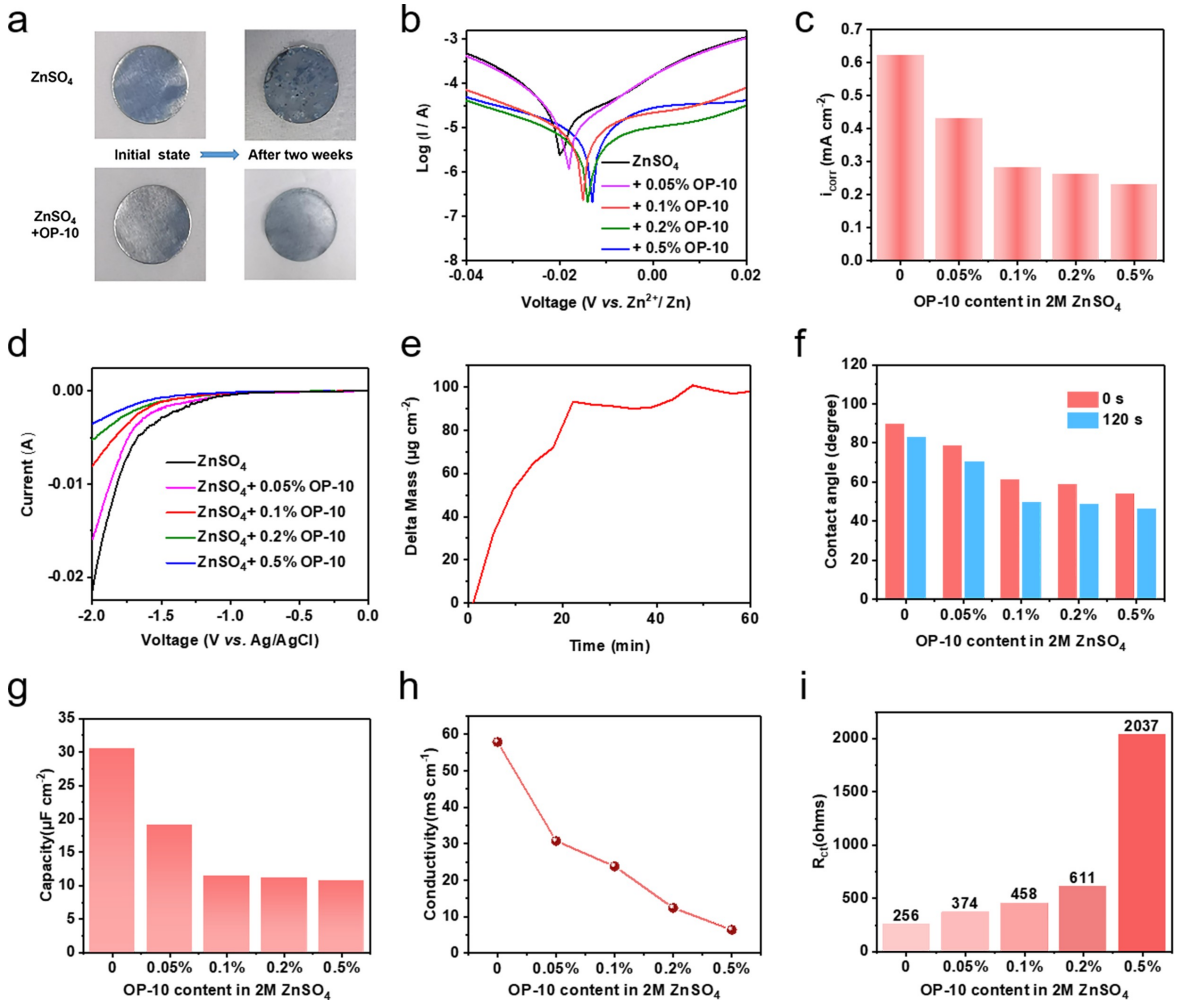

Figure 1. a) Optical images of the Zn-foil in its initial state and immersed in 2 M $ZnSO_4$ electrolytes with and without OP-10 for two weeks. b) The potentiodynamic polarization curves of the Zn foil in 2 M $ZnSO_4$ electrolytes and with added 0.05 wt%, 0.1 wt%, 0.2 wt%, 0.5 wt% OP-10 electrolytes. c) The corrosion current density (i_{corr}) of 2 M $ZnSO_4$ and with added 0.05 wt%, 0.1 wt%, 0.2 wt%, 0.5 wt% OP-10 electrolytes. d) HER of the electrolytes with different OP-10 concentrations. e) Delta mass of quartz sheet within 1 h . f) Contact angle analysis of 2 M $ZnSO_4$ and with added 0.05 wt%, 0.1 wt%, 0.2 wt%, 0.5 wt% OP-10 electrolytes on the Zn foil. g) EDLC of Zn anodes using Zn//Zn cell configurations in pure $ZnSO_4$ and with added 0.05 wt%, 0.1 wt%, 0.2 wt%, 0.5 wt% OP-10 electrolytes. h) The ionic conductivity of the electrolytes with different OP-10 concentrations. i) The charge-transfer resistance of the electrolytes with different OP-10 concentrations. (The OP-10 content is wt%, for simplicity, it is represented by % in the Figure, similarly hereinafter.)

affirming the strong adsorbability of OP-10 on Zn surface. The ether molecules' adsorption at the outer Zn anode surface was also verified in symmetrical Zn//Zn cells by the electric double-layer capacitance (EDLC).[38] As shown in Figures 1(g) and S4, the EDLC reduced in the following order: the pure $ZnSO_4$ electrolyte (30.5 μF cm^{-2}) > with 0.05 wt% OP-10(19 μF cm^{-2}) > with 0.1 wt% OP-10 (11.5 μF cm^{-2}) > with 0.2 wt% OP-10 (11.1 μF cm^{-2}) > with 0.5 wt% OP-10 (10.7 μF cm^{-2}), also demonstrating the excellent OP-10 absorbability. Which is worth less as the additional OP-10 amount increases from 0.1 wt% to 0.5 wt%, and the decrease of the contact angle and EDLC is not obvious. Combined with the above-mentioned experimental results, it is speculated that the adsorption of OP-10 on the surface of the zinc sheet reaches a state of saturation when the addition amount is about 0.1 wt%. An overdose of OP-10 will reduce the ionic conductivity (Figure 1h) and enhance the charge-transfer resistance (R_{ct}) (Figure 1i), which will undoubtedly cause severe polarization. Thus, a satisfactory addition amount was defined as 0.1 wt%, which is far lower than the reported addition amount of organic additives (Table S1).

To investigate the effect of OP-10 on reducing by-products, Zn//Zn symmetric cells were assembled using 2 M $ZnSO_4$ electrolyte with and without OP-10. Figure 2(a) shows the X-ray diffraction (XRD) of the zinc foil after 50 cycles at 1 mA cm^{-2}. There was $Zn_4SO_4(OH)_6 \cdot 4H_2O$ as a by-product in the zinc foil that was circulated 50 times in pure $ZnSO_4$ electrolyte. In contrast, almost no peak of the by-product was observed in the electrolyte with OP-10 additive. Further characterization of elemental composition was done by energy dispersive spectrometer (EDS) analysis, resulting depicted in Figure S5. Pure $ZnSO_4$ electrolyte may contain distinct S element, suggesting some by-products containing SO_4^{2-} formed on Zn-foil surface. Compared with pure $ZnSO_4$ electrolyte, the peaks of (002)

Research Article
doi.org/10.1002/batt.202200219
Chemistry Europe
European Chemical Societies Publishing

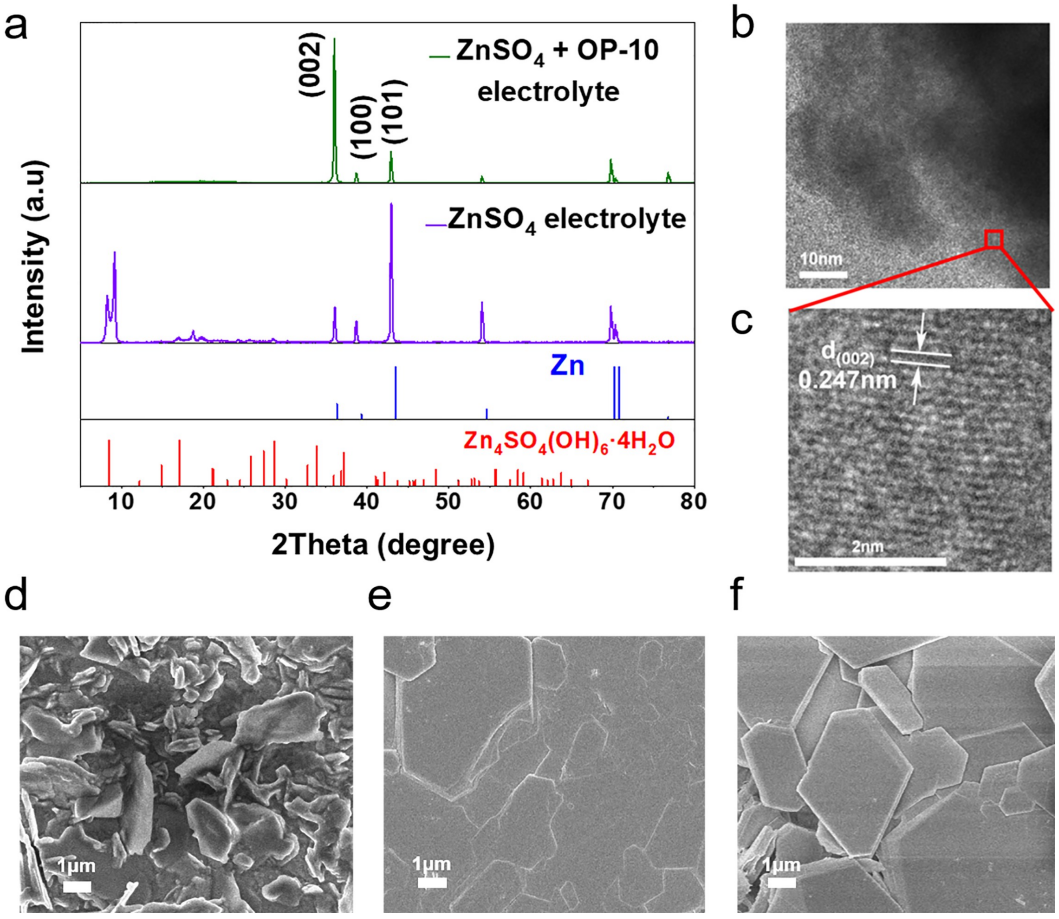

Figure 2. a) XRD patterns of the Zn foil in 2 M $ZnSO_4$ and $ZnSO_4$ + 0.1 wt% OP-10 electrolytes after 50 cycles. b, c) HRTEM images of the Zn foil in 2 M $ZnSO_4$ + OP-10 electrolytes after 50 cycles. d–f) SEM images of the Zn foil in 2 M pure $ZnSO_4$, $ZnSO_4$ + 0.1 wt% OP-10 and $ZnSO_4$ + 0.5 wt% OP-10 electrolytes after zinc stripping/plating 50 cycles, respectively.

crystal plane orientation increased significantly, while those of (100) and (101) crystal plane orientation decreased significantly in $ZnSO_4$ with OP-10 additive electrolyte. To further prove the crystallographic orientation of the Zn deposition process, Zn-foil circulated in $ZnSO_4$ with OP-10 additive electrolyte was observed under the high resolution transmission electron microscope (HRTEM) (Figure 2b). Interestingly, the Zn-foil deposit surface displays a crystal orientation that is homogeneous and has the same direction lattice fringes (Figure 2c), and the 0.247 nm lattice spacing can be identified as (002) plane of Zn.[20] The lowest energy (002) of Zn basal planes is parallel to the surface of zinc foil, which was conducive to the uniform deposition of Zn^{2+}.[39] The crystal orientation of zinc (100) and (101) is perpendicular to the surface of the zinc foil, and the interfacial charge density distribution was not uniform, leading to the uneven flux of $Zn^{2+}$and dendritic growth .[40] Numerous flake dendrites grew on the Zn-foil surface in pure $ZnSO_4$ electrolyte after 50 cycles, which were mostly perpendicular to the direction of zinc foil with the trend of aggregation and enlargement (Figure 2d). The zinc foil circulating in $ZnSO_4$ with 0.1 wt% OP-10 electrolyte shows an obvious trend of growth in a parallel direction (Figure 2e), and that in $ZnSO_4$ with 0.5 wt% OP-10 electrolyte is more inclined to be deposited as hexagonal planar sedimentary configuration (Figure 2f). Due to hexagonal close-packed (HCP) zinc crystal anisotropy, Zn preferentially uncovers the basal plane (002), having the highest atomic packing density, in order to reduce its surface free energy. That is the (002) Zn crystal direction which is parallel to the normal plane of the plate-like Zn electrodeposits.[41] In conclusion, OP-10 induced the growth orientation of zinc along the parallel direction, which promoted the uniform charge distribution on the surface of zinc foil, greatly reduced the growth of dendrite, and reduced the risk of dendrite penetrating separator short circuit.

Different proportions of additives had different degrees of influence on reversible Zn plating and stripping measurements. The most appropriate ratio was explored through electrochemical testing. The mass percentages of 0, 0.05, 0.1, 0.2, and 0.5 wt% were configured, the Zn//Zn symmetrical cell experiments for five batteries in each group were carried out, and the optimal data of each group were selected for comparison (Figure 3a). The cells assembled with pure $ZnSO_4$ and $ZnSO_4$ with 0.05 wt% OP-10 electrolyte were short-circuited at about 150 and 450 hours, respectively. When the amount of OP-10 was 0.5 wt%, the polarization voltage increased significantly compared with other electrolytes (pure $ZnSO_4$, with 0.1 wt%

Research Article
doi.org/10.1002/batt.202200219
Chemistry Europe
European Chemical Societies Publishing

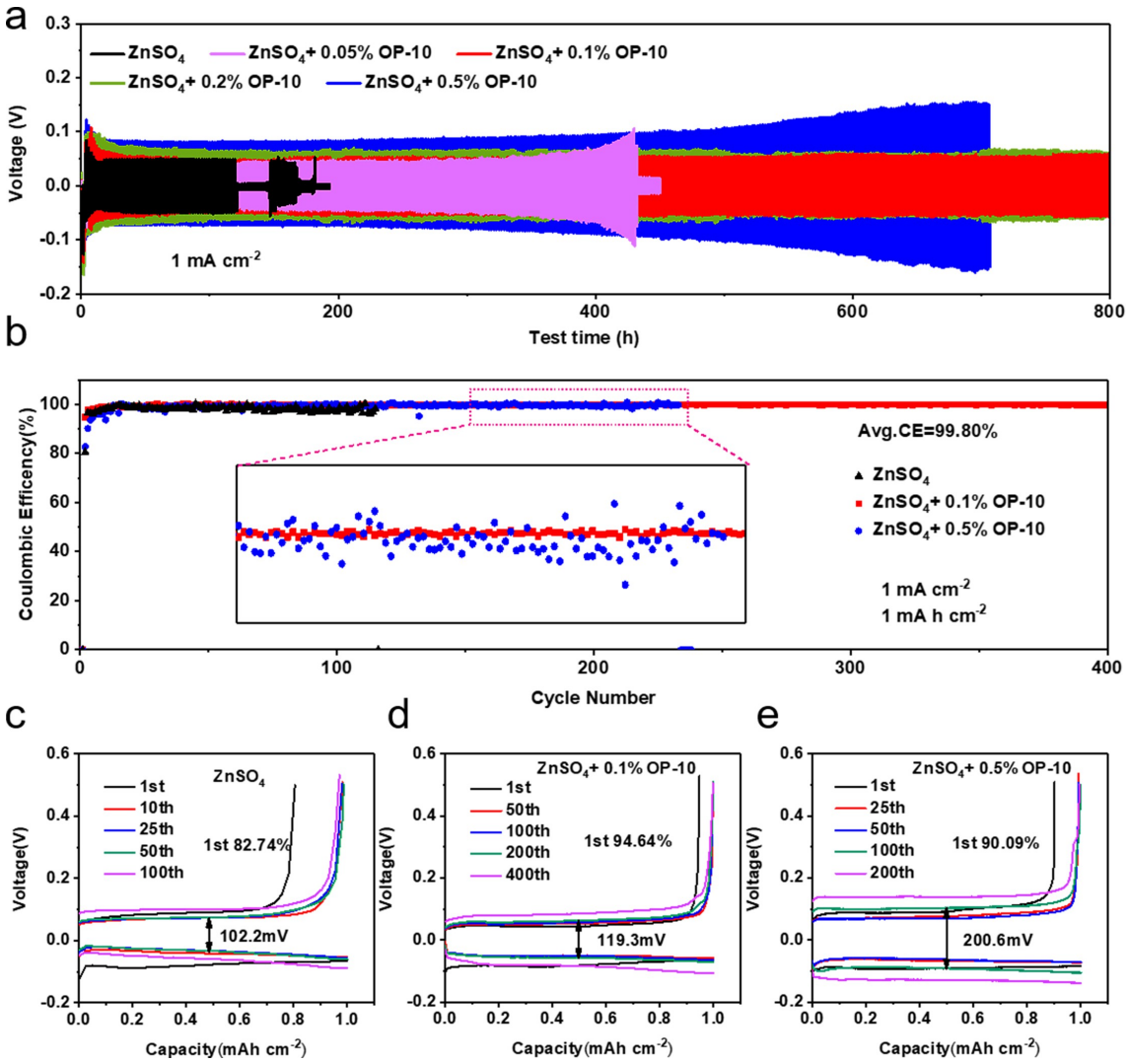

Figure 3. a) Galvanostatic cycling performance of Zn//Zn symmetric cell in 2 M pure $ZnSO_4$ and with added 0.05, 0.1, 0.2, 0.5 wt% OP-10 electrolytes at 1 mA cm^{-2} with 1 mAh cm^{-2}. b) Cycling performance of Zn//Cu cell in 2 M pure $ZnSO_4$ and with added 0.1 wt%, 0.5 wt% OP-10 electrolytes at 1 mA cm^{-2} with 1 mAh cm^{-2}. C–e) voltage profiles at various cycles of Zn//Cu cell using pure $ZnSO_4$, $ZnSO_4$ with 0.1 wt% OP-10, and $ZnSO_4$ with 0.5 wt% OP-10 electrolyte, respectively.

and 0.2 wt% OP-10 additives), and the cycle stability decreased. The polarization voltage of 0.1 wt% of the additive was lower than that of 0.2 wt% of the additive. In summary, the most suitable additive proportion of OP-10 is 0.1 wt%, and the symmetric cells show longed cycle life of over 800 hours at 1 mA cm^{-2} with 1 mAh cm^{-2}. The Coulombic efficiency (CE) is important for evaluating Zn reversibility during repeated cycling recorded by assembling Zn//Cu cell using $ZnSO_4$ with and without OP-10 additives and cycled with 1 mA h cm^{-2} plating capacity at 1 mA cm^{-2}, and then charged to 1 V (vs. Zn^{2+}/Zn) (Figure 3b). Unfortunately, the CE using the pure $ZnSO_4$ electrolyte was about 97.63% in only 98 cycles, possibly because of dendrites and side reactions. As compared with Zn//Cu, a cell that utilizes $ZnSO_4$ with 0.1 wt% OP-10 electrolyte, it attained an excellent and stable plating/stripping efficiency within 5 cycles and kept for over 400 cycles, with an average CE of 99.80%. In addition, the cycle life is longer and the stability is better compared with $ZnSO_4$ with 0.5 wt% OP-10 electrolyte. Figure 3(c–e) shows voltage profiles at various cycles. The initial CE of $ZnSO_4$ with 0.1 wt% OP-10 electrolyte (94.64%) was much higher than that of pure $ZnSO_4$ electrolyte (82.74%) and $ZnSO_4$ with 0.5 wt% OP-10 electrolyte (90.09%). Meanwhile, the initial voltage hysteresis of $ZnSO_4$ with 0.5 wt% OP-10 electrolyte was about 200 mV, which was higher than 102.2 mV of pure $ZnSO_4$ electrolyte and 119.3 mV of $ZnSO_4$ with 0.1 wt% OP-10 electrolyte. It indicates that 0.5 wt% OP-10 significantly reduced the reaction kinetics of the zinc foil surface, while 0.1 wt% OP-10 greatly improved the cyclic reversibility and stability of the zinc strip without reducing the kinetics. As a result, Zn//Cu cell using $ZnSO_4$ with 0.1 wt% OP-10 electrolyte can present much better cycling stability. Figure S6 shows the results of the chronoamperometry (CA) test. The CA curve of current for pure $ZnSO_4$ electrolyte, shows a continuous increase in tendency within 1000 s under and overpotential of −10 mV, demonstrating the unordered growth and nucleation of zinc. However, the $ZnSO_4$ with OP-10 is

Research Article
doi.org/10.1002/batt.202200219
Chemistry Europe
European Chemical Societies Publishing

maintained a stable current density after the increase in the early deposition stage for the coated-Zn foil.

Real-time observation of the Zn electrode surface with constant current deposition in the symmetrical cell showed the same results (Figure 4a, b). With 10 mA cm^{-2} current density, the deposition effect was significantly different with the extension of deposition time. After 15 min plating and dendrites, non-uniform nucleation sites for pure $ZnSO_4$ electrolyte occurred, which became visible after 25 min. However, the deposition process seemed to be uniform and stable for the $ZnSO_4$ with OP-10 electrolyte indicating that the addition of OP-10 was conducive to the uniform distribution of nucleation sites on the surface of the zinc foil and inhibited the growth of zinc dendrite. According to the previous experimental, the OP-10 additive inhibition of zinc dendrite overall mechanism is shown in Figure 4(c and d). The coordination of H_2O of $Zn(H_2O)_6^{2+}$ molecule is easy to decompose to H_2 and OH^-, resulting in the formation of $Zn_4SO_4(OH)_6 \cdot 4H_2O$ and other insulating materials in the local alkaline environment. The adsorption of precipitated gas on the Zn foil surface hindered the nucleation of zinc, which resulted in the uneven distribution of interfacial electric field and the increase of over potential, making it easier to form dendrites in the presence of the tip effect.[42] In contrast, OP-10 absorbs on the Zn-foil surface before dendritic growth, thereby shielding the cutting-edge electric field and regulating their absorbed concentration in accordance with the deposited electrode's surface curvature,[43] these factors together aid in constant concave

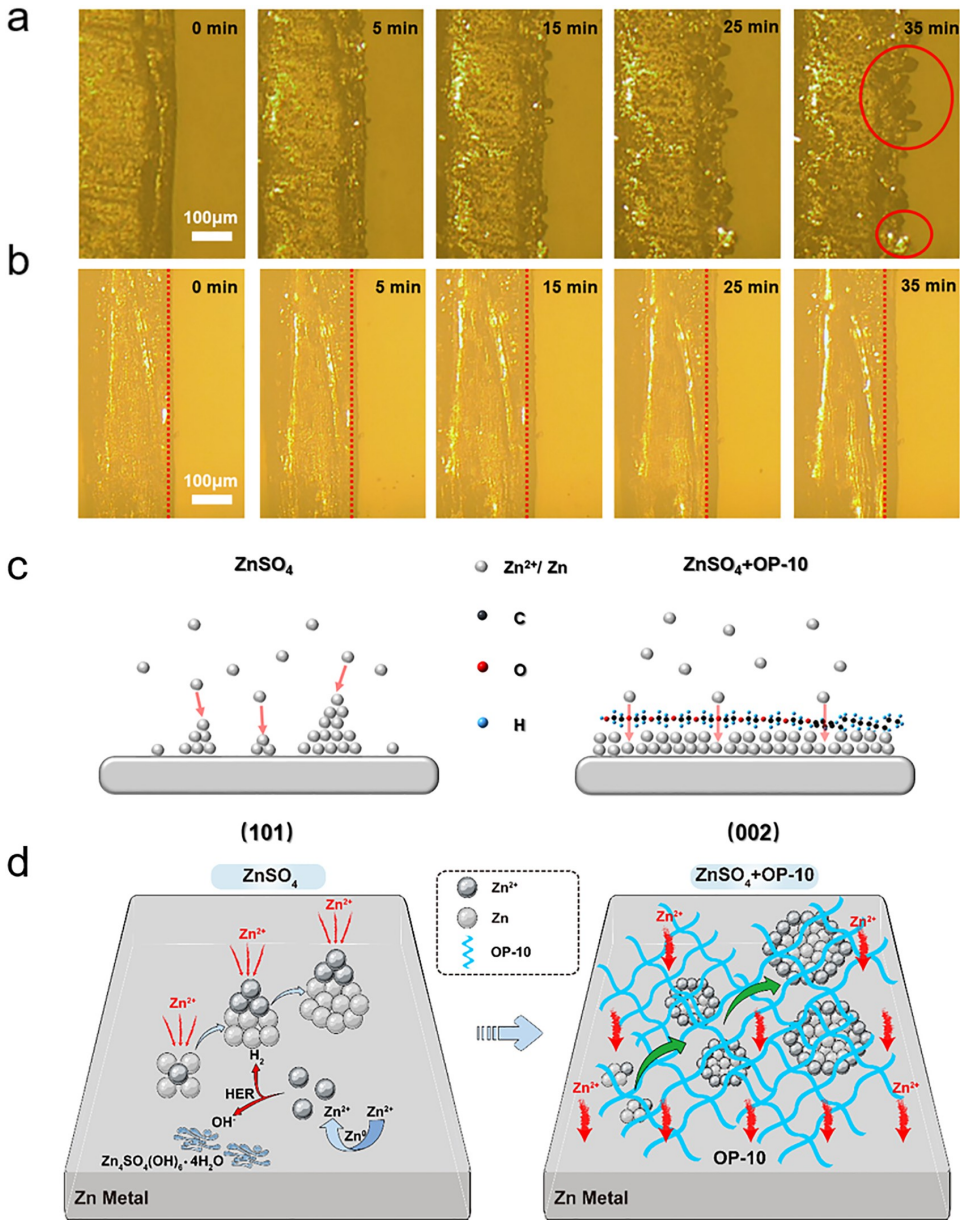

Figure 4. The results of in situ optical observation of Zn deposition morphologies on Zn foil in a) 2 M pure $ZnSO_4$ and $ZnSO_4$ with 0.1 wt% OP-10 electrolytes, b) at a current density of 10 mA cm^{-2} for 35 min. c and d) Schematic diagram of the mechanism of OP-10 for suppressing Zn dendrite.

Research Article
doi.org/10.1002/batt.202200219
Chemistry Europe
European Chemical Societies Publishing

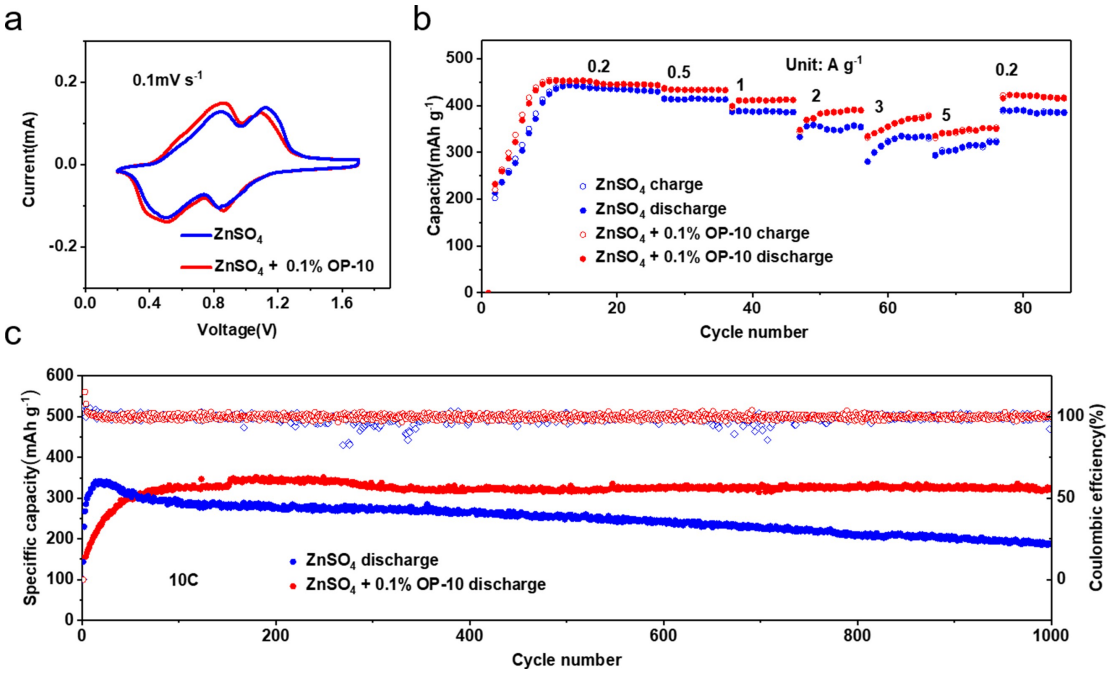

Figure 5. Performance comparison of Zn//$V_2O_5 \cdot 1.6H_2O$ full cell between pure $ZnSO_4$ and $ZnSO_4$ with 0.1 wt% OP-10. a) CV measurement of Zn//$V_2O_5 \cdot 1.6H_2O$ battery. b) Rate capacities under various current densities ranging from 0.2 to 5 A g^{-1}. c) The cycling performance at 10 C (1 C = 589 mA g^{-1}).

surface filling and level up the upper surface for the deposition of Zn atom. This behavior is called a super-filling phenomenon and it has already been proposed.[44] A large number of zincphilic groups of OP-10 increase the nucleation sites, which can homogenize Zn^{2+} cations transport toward the electrode surface and hence, stabilizes the electrodeposition in a regime below a critical flux.[36] This change is beneficial to the deposition and growth of zinc in the direction parallel to the zinc foil, making the Zn (002) planes dominant and displaying a key role in inhibiting Zn dendrite growth.[39] Concurrently, the adsorption of OP-10 on the Zn-foil surface also reduces the coordinated water molecules from direct contact with the electrode surface, thereby preventing the decomposition of water and other side reactions. In summary, OP-10 played an obvious role in inhibiting the growth of zinc dendrite and the generation of side reactions.

Finally, Zn//$V_2O_5 \cdot 1.6H_2O$ battery based on $V_2O_5 \cdot 1.6H_2O$ cathode (Figures S7 and S8) and Zn-foil anode was created to confirm the availability of the OP-10 additives. CV curves of the Zn//$V_2O_5 \cdot 1.6H_2O$ battery show that both present two pairs of catholic/anodic peaks corresponding to the two-step reverse oxidation/reduction between V^{5+} and V^{3+} (Figure 5a). It is significant to note that redox peaks of Zn//$V_2O_5 \cdot 1.6H_2O$ battery with different electrolytes are barely shifted, indicating that a small amount of OP-10 has almost no effect on the polarization voltage. Compared with pure $ZnSO_4$ electrolyte, the overall Zn//$V_2O_5 \cdot 1.6H_2O$ battery performance was effectively enhanced by incorporating minute levels of OP-10 to the $ZnSO_4$ electrolyte. As shown in Figure 5(b), compared with using pure $ZnSO_4$ electrolyte, using $ZnSO_4$ with OP-10 electrolyte has better rate performance. In addition, the Zn//$V_2O_5 \cdot 1.6H_2O$ battery using $ZnSO_4$ with OP-10 electrolyte can support an extensive cycle lifespan with higher stability (approximately 92.12% retention post 1000 cycles) compared to those using pure $ZnSO_4$ electrolyte (58.34% post 1000 cycles) at 10 C (Figure 5c). A similar phenomenon was observed at 0.5 C (Figure S9). These results suggest that the OP-10 additive can efficiently reduce the parasitic reactions between the electrolyte and Zn-anode and assists a uniform Zn nuclei distribution favoring long-term cycling stability.

Conclusion

In conclusion, an ultralow amount of (0.1 wt%) of OP-10 in the $ZnSO_4$ electrolyte improved the performance of the zinc ion battery. It is presumed that the firm adsorption of OP-10 on the Zn-anode can efficiently influence the initial Zn^{2+} ions to deposit through a regular hexagonal (002) plane. The depositions of these exposing (002) plane possess superior ability towards Zn atoms catching and the characteristic of even interfacial charge distribution facilitate the growth of deposited zinc with the same preferential orientation, which eventually leads to the formation of the compact plating layer. The deposition and growth of zinc ions tended to the advantages (002) crystal plane, which induces the uniform deposition of zinc and greatly reduces the growth of dendrites and the generation of by-products. The most suitable dosage of OP-10 additive is about 0.1 wt% by mass, which was lower than most of the additives previously reported. It not only saved cost but also increases the energy density of the battery, which is more in line with the modification idea of "small dose and large effect" of additives.

Experimental Section

Preparation of $V_2O_5 \cdot 1.6H_2O$ cathode

$V_2O_5 \cdot 1.6H_2O$ was synthesized by a hydrothermal method. Typically, 0.91 g V_2O_5 powder, 12.5 mL H_2O_2 (30 wt%) and 75 mL deionized water were mixed to obtain a clear orange solution. Subsequently, the mixture was transferred into Teflon-lined stainless steel autoclave and heated at 190 °C for 20 h. The final product was obtained after freeze-drying.

Characterization

XRD patterns were collected using a Rigaku MiniFlex600 with Cu Kα radiation and the zinc plate was washed by deionized water before XRD tests. The microstructure and morphology were observed by field-emission scanning electron microscopy (SEM, JEOL JSM7500F) and high resolution transmission electron microscopy (HRTEM, Talos F200X G2) equipped with energy dispersive spectroscopy (EDS) for elemental analysis. Contact angles were conducted by using a contact angle measurement (Data physics, TBU 100).

Electrochemical measurement

The linear sweep voltammetry (LSV) experiment were conducted using a three-electrode system (Ti as working electrode and the counter electrode, and Ag/AgCl as the reference electrode) and the scan rate is 10 mV s^{-1}. The V_2O_5 electrodes were prepared by mixing $V_2O_5 \cdot 1.6H_2O$, Ketjen black (KB), and Polytetrafluoroethylene (PTFE) at a weight ratio of 7:2:1, and presses onto titanium mesh (the mass load is about 2–3 mg cm^{-2}). Then the electrode films were dried at 80 °C for 12 h under vacuum. The $Zn//V_2O_5 \cdot 1.6H_2O$ battery was assembled in CR2032-type, using zinc foil as anode (the thickness and diameter of zinc foil are 0.05 mm and 12 mm, respectively), glass fiber filter as the separator, and $V_2O_5 \cdot 1.6H_2O$ electrodes as cathode. Taking into the consumption of zinc during the battery cycles, the mass of zinc used was excessive for the match of cathode/anode ratio. CV tests were performed using a CHI660E electrochemical workstation (ChenHua, Shanghai, China). The galvanostatic discharge/charge tests were performed on a LAND-CT2001 A battery testing system.

Calculation details

The ionic conductivity is calculated following the equation:

$$\sigma = L/RS,$$

where σ is the ionic conductivity; L the thicknesses of the electrolyte; R the resistance of the electrolyte; S the area of the electrolyte.

Electrochemical quartz crystal microbalance (EQCM) has emerged as a very powerful "in situ" technique to determine the mass change of film deposited on electrode. Quartz is one of the materials with piezoelectric properties, the mass change of film is correlated with the frequency through a simple Sauerbrey equation:

$$\Delta f = -2f_0^2 \Delta m / A\left(\mu_q \rho_q\right)^{1/2}$$

where $\triangle f$ is the measured frequency shift, f_0 the frequency of the quartz crystal prior to a mass change, $\triangle m$ the mass change, A the piezoelectrically active area, μ_q the density of quartz, and ρ_q the shear modulus.

Acknowledgements

This study was supported the National Natural Science Foundation of China (51771094 and 21835004), the National Key R&D Program of China (2016YFB0901500), Ministry of Education of China (B12015 and IRT13R30), and Tianjin Natural Science Foundation (No. 18JCZDJC31500). We thank the Haihe Laboratory of Sustainable Chemical Transformations for financial support. The work was carried out at Shanxi Supercomputing Center of China, and the calculations were performed on TianHe-2.

Conflict of Interest

The authors declare no conflict of interest.

Data Availability Statement

Research data are not shared.

Keywords: aqueous zinc-ion batteries · crystal growth orientation · electrolyte · OP-10 additive · small dose

[1] D. Chao, W. Zhou, F. Xie, C. Ye, H. Li, M. Jaroniec, S. Z. Qiao, *Sci. Adv.* **2020**, *6*, eaba4098.
[2] T. J. Sun, H. H. Du, S. B. Zheng, J. Q. Shi, Z. L. Tao, *Adv. Funct. Mater.* **2021**, *31*, 2010127.
[3] Z. X. Liu, L. P. Qin, B. G. Lu, X. W. Wu, S. Q. Liang, J. Zhou, *ChemSusChem* **2022**, *15*, e202200348.
[4] J. Shin, J. Lee, Y. Park, J. W. Choi, *Chem. Sci.* **2020**, *11*, 2028–2044.
[5] Z. Y. Cao, X. D. Zhu, D. X. Xu, P. Dong, M. O. L. Chee, X. J. Li, K. Y. Zhu, M. X. Ye, J. F. Shen, *Energy Storage Mater.* **2021**, *36*, 132–138.
[6] Q. Zhang, J. Luan, X. Huang, Q. Wang, D. Sun, Y. Tang, X. Ji, H. Wang, *Nat. Commun.* **2020**, *11*, 3961.
[7] H. Jia, Z. Q. Wang, B. Tawiah, Y. D. Wang, C. Y. Chan, B. Fei, F. Pan, *Nano Energy* **2020**, *70*, 104523.
[8] M. Song, H. Tan, D. L. Chao, H. J. Fan, *Adv. Funct. Mater.* **2018**, *28*, 1802564.
[9] Q. Zhang, J. Luan, L. Fu, S. Wu, Y. Tang, X. Ji, H. Wang, *Angew. Chem. Int. Ed. Engl.* **2019**, *58*, 15841–15847.
[10] A. Bayaguud, Y. Fu, C. Zhu, *J. Energy Chem.* **2022**, *64*, 246–262.
[11] C. Han, W. J. Li, H. K. Liu, S. X. Dou, J. Z. Wang, *Nano Energy* **2020**, *74*, 104880.
[12] J. W. Wang, Y. Yang, Y. X. Zhang, Y. M. Li, R. Sun, Z. C. Wang, H. Wang, *Energy Storage Mater.* **2021**, *35*, 19–46.
[13] P. C. Ruan, S. Q. Liang, B. G. Lu, H. J. Fan, J. Zhou, *Angew. Chem. Int. Ed.* **2022**, *61*, e202200598.
[14] Y. Yang, C. Liu, Z. Lv, H. Yang, Y. Zhang, M. Ye, L. Chen, J. Zhao, C. C. Li, *Adv. Mater.* **2021**, *33*, e2007388.
[15] H. B. He, H. Tong, X. Y. Song, X. P. Song, J. Liu, *J. Mater. Chem. A* **2020**, *8*, 7836–7846.
[16] X. H. Zeng, K. X. Xie, S. L. Liu, S. L. Zhang, J. N. Hao, J. Liu, W. K. Pang, J. W. Liu, P. H. Rao, Q. H. Wang, J. F. Mao, Z. P. Guo, *Energy Environ. Sci.* **2021**, *14*, 5947–5957.
[17] Y. Tian, Y. L. An, C. K. Liu, S. L. Xiong, J. K. Feng, Y. T. Qian, *Energy Storage Mater.* **2021**, *41*, 343–353.
[18] Y. Zeng, X. Zhang, R. Qin, X. Liu, P. Fang, D. Zheng, Y. Tong, X. Lu, *Adv. Mater.* **2019**, *31*, e1903675.

[19] C. Li, Z. Sun, T. Yang, L. Yu, N. Wei, Z. Tian, J. Cai, J. Lv, Y. Shao, M. H. Rummeli, J. Sun, Z. Liu, *Adv. Mater.* **2020**, *32*, e2003425.
[20] J. Cao, D. D. Zhang, C. Gu, X. Wang, S. M. Wang, X. Y. Zhang, J. Q. Qin, Z. S. Wu, *Adv. Energy Mater.* **2021**, *11*, 2101299.
[21] H. P. Li, C. Guo, T. S. Zhang, P. Xue, R. Z. Zhao, W. H. Zhou, W. Li, A. Elzatahry, D. Y. Zhao, D. L. Chao, *Nano Lett.* **2022**, *22*, 4223–4231.
[22] B. Y. Zhang, L. P. Qin, Y. Fang, Y. Z. Chai, X. S. Xie, B. G. Lu, S. Q. Liang, J. Zhou, *Sci. Bull.* **2022**, *67*, 955–962.
[23] H. H. Du, K. Wang, T. J. Sun, J. Q. Shi, X. Z. Zhou, W. Cai, Z. L. Tao, *Chem. Eng. J.* **2022**, *427*, 131705.
[24] Y. Y. Wang, Z. J. Wang, F. H. Yang, S. L. Liu, S. L. Zhang, J. F. Mao, Z. P. Guo, *Small* **2022**, 2107033.
[25] S. L. Liu, R. Z. Zhang, J. F. Mao, Y. L. Zhao, Q. Cai, Z. P. Guo, *Sci. Adv.* **2022**, *8*, eabn5097.
[26] S. L. Liu, J. F. Mao, W. K. Pang, J. Vongsvivut, X. H. Zeng, L. Thomsen, Y. Y. Wang, J. W. Liu, D. Li, Z. P. Guo, *Adv. Funct. Mater.* **2021**, *31*, 2104281.
[27] J. Q. Shi, T. J. Sun, J. Q. Bao, S. B. Zheng, H. H. Du, L. Li, X. M. Yuan, T. Ma, Z. L. Tao, *Adv. Funct. Mater.* **2021**, *31*, 2102035.
[28] W. N. Xu, K. N. Zhao, W. C. Huo, Y. Z. Wang, G. Yao, X. Gu, H. W. Cheng, L. Q. Mai, C. G. Hu, X. D. Wang, *Nano Energy* **2019**, *62*, 275–281.
[29] P. Sun, L. Ma, W. Zhou, M. Qiu, Z. Wang, D. Chao, W. Mai, *Angew. Chem. Int. Ed. Engl.* **2021**, *60*, 18247–18255.
[30] A. Mitha, A. Z. Yazdi, M. Ahmed, P. Chen, *ChemElectroChem* **2018**, *5*, 2409–2418.
[31] S. J. Banik, R. Akolkar, *Electrochim. Acta* **2015**, *179*, 475–481.
[32] T. Y. Zhou, Y. L. Mu, L. Chen, D. X. Li, W. Liu, C. K. Yang, S. B. Zhang, Q. Wang, P. Jiang, G. L. Ge, H. H. Zhou, *Energy Storage Mater.* **2022**, *45*, 777–785.
[33] K. E. Sun, T. K. Hoang, T. N. Doan, Y. Yu, X. Zhu, Y. Tian, P. Chen, *ACS Appl. Mater. Interfaces* **2017**, *9*, 9681–9687.
[34] D. H. Zhang, A. J. Warren, G. J. Li, Z. Cheng, X. X. Han, Q. Zhao, X. T. Liu, Y. Deng, L. Archer, *Macromolecules* **2020**, *53*, 2694–2701.
[35] M. Haataja, D. J. Srolovitz, *Phys. Rev. Lett.* **2002**, *89*, 215509.
[36] A. R. Rajamani, S. Jothi, M. Datta, M. Rangarajan, *J. Electrochem. Soc.* **2018**, *165*, D50-D57.
[37] D. A. Buttry, M. D. Ward, *Chem. Rev.* **1992**, *92*, 1355–1379.
[38] L. M. Da Silva, L. A. De Faria, J. F. C. Boodts, *Electrochim. Acta* **2001**, *47*, 395–403.
[39] J. Zheng, L. A. Archer, *Sci. Adv.* **2021**, *7*, eabe0219.
[40] M. Zhou, S. Guo, J. Li, X. Luo, Z. Liu, T. Zhang, X. Cao, M. Long, B. Lu, A. Pan, G. Fang, J. Zhou, S. Liang, *Adv. Mater.* **2021**, *33*, e2100187.
[41] J. Zheng, J. Yin, D. Zhang, G. Li, C. Bock David, T. Tang, Q. Zhao, X. Liu, A. Warren, Y. Deng, S. Jin, C. Marschilok Amy, S. Takeuchi Esther, J. Takeuchi Kenneth, D. Rahn Christopher, A. Archer Lynden, *Sci. Adv.* **2021**,*6*, eabb1122.
[42] X. X. Guo, Z. Y. Zhang, J. W. Li, N. J. Luo, G. L. Chai, T. S. Miller, F. L. Lai, P. Shearing, D. J. L. Brett, D. L. Han, Z. Weng, G. J. He, I. P. Parkin, *ACS Energy Lett.* **2021**, *6*, 395–403.
[43] T. Wang, Y. Li, J. Zhang, K. Yan, P. Jaumaux, J. Yang, C. Wang, D. Shanmukaraj, B. Sun, M. Armand, Y. Cui, G. Wang, *Nat. Commun.* **2020**, *11*, 5429.
[44] D. Josell, T. P. Moffat, D. Wheeler, *J. Electrochem. Soc.* **2007**, *154*, D208-D214.

Manuscript received: May 12, 2022
Revised manuscript received: June 20, 2022
Accepted manuscript online: June 21, 2022
Version of record online: July 4, 2022